Co-Simulation of a Printed Circuit Board Modeled by a Cauer Ladder Network Approach Combined With GaN Transistors

Thomas Henneron, Wei Chen, Loris Pace, Jérôme Tomezyk, Stéphane Clénet, and Houssein Taha

***Abstract*—In order to design efficient power converter operating at high switching frequencies, the electromagnetic behavior of the printed circuit board (PCB) must be well known. Then, numerical approaches can be used to study the voltage and current waveforms as well as the current density distribution associated with a PCB. Considering a half-bridge converter connected to a passive electrical load, we propose a co-simulation based on the Cauer ladder network approach providing an equivalent circuit of the PCB combined with models of GaN transistors. The results from the co-simulation are compared with measurements at 1 MHz with an output power of 200 W.**

***Index Terms*—Cauer ladder network (CLN), co-simulation, finite element (FE) method, GaN transistors, high frequency power converters, model order reduction.**

I. Introduction

DUE to the development of semiconductors used in power converters, switching frequencies become increasingly significant. Then, the influence of the electromagnetic behavior associated with the PCB cannot be neglected with regard to semiconductors and/or passive components during the design phase of a converter. To study the behavior of a PCB, numerical approaches can be investigated. In the literature, the Partial Element Equivalent Circuit (PEEC) modeling method is commonly used to determine a differential equation system based on global electrical quantities (currents and electric potentials) [1], [2], [3]. The PEEC approach does not require meshing the air surrounding a conductive subdomain but it does result in a dense matrix system that needs to be solved. For a magneto-quasistatic problem in the frequency domain, the PEEC approach defines an equivalent circuit composed of resistors and inductances depending on the frequency. In order to study the transient state in the time domain, approaches such as Vector Fitting, Inverse Fourier Transform, or numerical inversion of the Laplace Transform can be performed with the frequency dependent matrix system in order to obtain an equivalent circuit with constant resistors and inductances [1]. Then, a co-simulation based on solving of the equivalent circuit combined with semiconductors and/or passive components can be performed. Another approach is to use the Marching On–in–Time PEEC method to directly define an equivalent circuit with constant parameters [4], which requires the introduction of temporal shape functions.

The finite element (FE) method can also be investigated to study the electromagnetic behavior of a PCB [5]. However, the approach requires meshing the whole studied domain. To avoid meshing the conductive tracks, which are essentially 2-D surfaces, Shell element approaches can be employed [6]. In the literature, this approach has been investigated to study the electromagnetic behavior of two different PCB designs [7]. In the case of a co-simulation, the FE model is coupled with models of semiconductors and/or passive components. Nevertheless, due to the computational time required to solve the FE model, which depends on meshing the entire domain, this approach is typically not used for real applications.

In this article, the Cauer ladder network (CLN) approach is applied to the magneto-quasistatic FE model of a PCB in order to define an equivalent circuit composed of resistors and inductances. The CLN approach is a model order reduction method which enables to derive a numerical model with a small number of unknowns from the FE model [8]. The unknowns of the model are then the currents and the voltages of the equivalent circuit. The CLN method has been proposed by [8] and applied to a 2-D magneto-quasistatic problem solved by a potential formulation. This approach consists of two main steps. During the offline step, based on a FE model, an equivalent electrical circuit composed of resistors and inductances as well as a reduced basis associated with the potential are defined. The online step involves solving the equivalent CLN circuit. The CLN approach enables an easy coupling with other equivalent circuit models of other components than the one modeled by the FE method. Moreover, is enables to calculate very quickly global quantities like, losses or fluxes as well as field distributions (current density, magnetic field...). This method has been extended for 3-D magneto-quasistatic [9], [10] and electro-quasistatic problems [11] and has been applied to numerous applications likes cables, transformers, electrical machines, but not to PCB until now.

Received 31 July 2024; revised 24 October 2024 and 20 December 2024; accepted 15 January 2025. Date of publication 17 January 2025; date of current version 26 February 2025. Recommended for publication by Associate Editor S. Y. R. Hui. *(Corresponding author: Thomas Henneron.)*

Thomas Henneron, Wei Chen, Jérôme Tomezyk, Stéphane Clénet, and Houssein Taha are with the University Lille, Arts et Métiers Institute of Technology, F-59000 Lille, France (e-mail: thomas.henneron@univ-lille.fr).

Loris Pace is with the Ecole Centrale de Lyon, University Claude Bernard Lyon 1, 69130 Ecully, France.

Color versions of one or more figures in this article are available at https://doi.org/10.1109/TPEL.2025.3531205.

Digital Object Identifier 10.1109/TPEL.2025.3531205

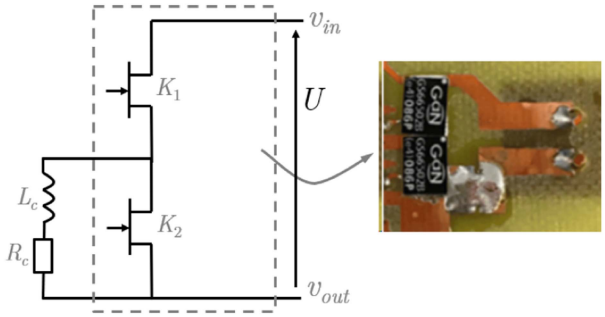

Fig. 1. Studied system.

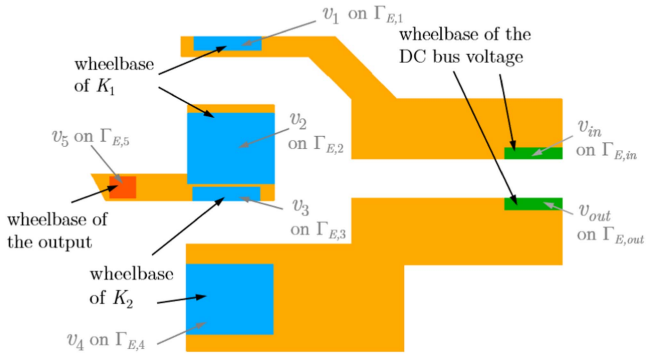

Fig. 2. Conductive subdomain D_c.

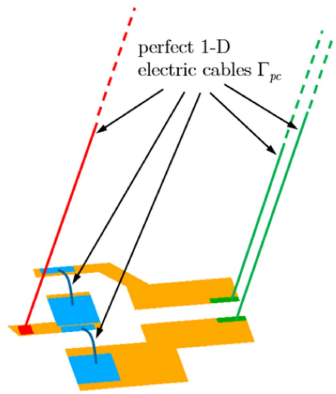

Fig. 3. Conductive subdomain with the perfect 1-D electric cables.

Based on a real half-bridge converter supplying a passive electrical load [12], the equivalent CLN circuit of the PCB is combined with models of GaN transistors to perform a co-simulation. The results from the co-simulation are compared with measurements. In a first part, the studied system is introduced. The second part details the numerical model of the PCB using FE approach. In a third part, the principle of the CLN method is presented and then applied to derive an equivalent electrical circuit of the PCB. In a fourth part, the results obtained from the equivalent CLN circuit are compared with those from the FE model, where transistors are substituted with ideal switches modeled by variable resistors. Finally, the results of a co-simulation using the equivalent CLN circuit of the PCB combined with PSICE models of GaN transistors are compared with measurements.

II. Studied System Based on a Half-Bridge Converter

The studied system is based on a half-bridge converter supplying an electrical load composed of a resistor R_c and an inductance L_c (Fig. 1). The converter is composed of two GaN transistors, K_1 and K_2, connected to the PCB. A comprehensive description of the system can be found in [12].

In this work, the switching frequency is fixed to $f = 1$ MHz, the duty cycle to 0.5 and the voltage U of the dc bus to 180 V.

III. Numerical Model of the PCB

A. Continuous Formulation

To take into account the resistive and inductive effects of the PCB, a magneto-quasistatic problem is considered. The PCB, excluding the conductive tracks connected to the transistor gates, forms a conductive subdomain D_c of boundary Γ_{D_c} with $\Gamma_{D_c} = \Gamma_E \bigcup \Gamma_J$ and $\Gamma_E \bigcap \Gamma_J = \emptyset$. The wheelbases of the transistors (drain and source), cables of the dc bus voltage and electrical load are taken into account. Each wheelbase corresponds to a boundary $\Gamma_{E,j} \in \Gamma_E$ where the electric scalar potential v_j is constant. The voltage U of the dc bus is defined by $U = v_{in} - v_{out}$, the drain-source voltage $V_{ds,1}$ of the transistor K_1 by $V_{ds,1} = v_1 - v_2$, $V_{ds,2} = v_3 - v_4$ for the transistor K_2 and the voltage U_c applied to the load by $U_c = v_5 - v_{out}$ (Fig. 2). Then, the boundary Γ_E can be split such as $\Gamma_E = \Gamma_{E,in} \bigcup \Gamma_{E,out} \bigcup \Gamma_{E,1} \bigcup \Gamma_{E,2} \bigcup \Gamma_{E,3} \bigcup \Gamma_{E,4} \bigcup \Gamma_{E,5}$.

The studied domain D of boundary Γ_D is composed of the subdomain D_c enclosed within an air box. To impose the conservation of the currents, perfect 1-D electric cables are introduced between $\Gamma_{E,in}$ and Γ_D, $\Gamma_{E,out}$ and Γ_D, $\Gamma_{E,5}$ and Γ_D, $\Gamma_{E,1}$ and $\Gamma_{E,2}$ and $\Gamma_{E,3}$ and $\Gamma_{E,4}$ (Fig. 3) [7]. The set of perfect 1-D cables are denoted by Γ_{pc}.

By neglecting the displacement currents, a magneto-quasistatic (MQS) problem is defined by

$$\mathbf{curl}\ \mathbf{E} = -\frac{\partial \mathbf{B}}{\partial t} \tag{1}$$

$$\mathbf{curl}\ \mathbf{H} = \mathbf{J} \tag{2}$$

$$div\mathbf{B} = 0 \tag{3}$$

$$div\mathbf{J} = 0 \tag{4}$$

with $\mathbf{E}$ the electric field, $\mathbf{B}$ the magnetic flux density, $\mathbf{H}$ the magnetic field, and $\mathbf{J}$ the current density in D_c. For the conductive tracks, the electric behavior law is $\mathbf{J} = \sigma\mathbf{E}$ with σ the conductivity. In the whole domain D, the magnetic behavior law is defined by $\mathbf{B} = \mu_0\mathbf{H}$ with μ_0 the permeability of the vacuum. To solve the problem, the $\mathbf{A} - v$ formulation can be used. A magnetic vector potential $\mathbf{A}$ is defined in the whole domain D from (3)

$$\mathbf{B} = \mathbf{curl}\mathbf{A} \text{ with } \mathbf{A} \times \mathbf{n} = \mathbf{0} \text{ on } \Gamma_D, \Gamma_E \text{ and } \Gamma_{pc} \tag{5}$$

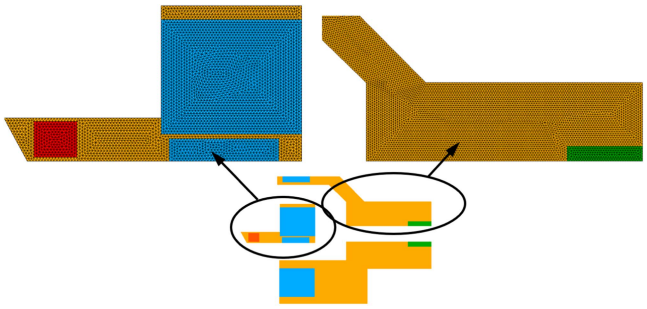

Fig. 4. Part of the PCB mesh.

with $\mathbf{n}$ the outward normal. From (1), the electric field can be expressed by

$$\mathbf{E} = -\frac{\partial \mathbf{A}}{\partial t} - \mathbf{grad}v - \sum_j v_j \mathbf{grad}\alpha_j$$
$$\text{with } j \in \{in, out, 1, 2, 3, 4, 5\} \text{ and } v = 0 \text{ on } \Gamma_E \quad (6)$$

where v is an electric scalar potential defined in the subdomain D_c and α_j is a scalar function equal to 1 on $\Gamma_{E,j}$ and 0 everywhere else, for $j \in \{in, out, 1, 2, 3, 4, 5\}$. Then, based on (2) and (4), the strong formulation to be solved is

$$\mathbf{curl}\nu\mathbf{curl}\mathbf{A} + \sigma\left(\frac{\partial \mathbf{A}}{\partial t} + \mathbf{grad}v + \sum_j v_j \mathbf{grad}\alpha_j\right) = \mathbf{0}, \quad (7)$$

$$div\sigma\left(\frac{\partial \mathbf{A}}{\partial t} + \mathbf{grad}v + \sum_j v_j \mathbf{grad}\alpha_j\right) = 0,$$
$$\text{with } \nu = 1/\mu_0 \text{ and } j \in \{in, out, 1, 2, 3, 4, 5\}. \quad (8)$$

The current i_k flowing through each boundary $\Gamma_{E,k}$ can be expressed by [13]

$$i_k = \int_{D_c} \sigma\left(\frac{\partial \mathbf{A}}{\partial t} + \mathbf{grad}v + \sum_j v_j \mathbf{grad}\alpha_j\right) \cdot \mathbf{grad}\alpha_k dD. \quad (9)$$

B. Finite Element (FE) Model

To optimize the discretization of the studied domain, the mesh of the PCB is based on a shell element method. This approach represents the thin structures as 2-D surfaces [6], [7]. Then, the conductive tracks are discretized using 90 749 triangular elements. The 3-D mesh for the remainder of studied domain consists of 285 644 tetrahedral elements. Fig. 4 presents a portion of the PCB mesh.

Based on Whitney's elements, the potentials $\mathbf{A}$ and v are discretized using edge and nodal elements, respectively, and the scalar functions α_j using the nodal elements [14]. We denote by $\mathbf{X}_A$ of size N_e the vector of degrees of freedom (DoF) of $\mathbf{A}$ and by $\mathbf{X}_v$ of size N_n the vector of DoF of v. The DoF numbers of $\mathbf{X}_A$ and $\mathbf{X}_v$ are about 370k and 33k, respectively. Then, we have

$$\mathbf{A} = \sum_{i=1}^{N_e} X_{A_i} \mathbf{w}_i^1(\mathbf{x}), \quad (10)$$

$$v = \sum_{i=1}^{N_n} X_{v_i} w_i^0(\mathbf{x}), \quad (11)$$

$$\alpha_j = \sum_{i \in \Gamma_{E,j}} w_i^0(\mathbf{x}) \quad (12)$$

with X_{A_i} the ith component of $\mathbf{X}_A$ which corresponds to the circulation of $\mathbf{A}$ along the edge i and $\mathbf{w}_i^1(\mathbf{x})$ its edge interpolation function depending on the position $\mathbf{x}$ and X_{v_i} the ith component of $\mathbf{X}_v$ which corresponds to the value of v on the node i and $w_i^0(\mathbf{x})$ its nodal interpolation function. Applying the FE method to (7) and (8) leads to the following system of equations to be considered:

$$\mathbf{M}_{AA}^{\nu}\mathbf{X}_A + \mathbf{N}_{AA}^{\sigma}\frac{d\mathbf{X}_A}{dt} + \mathbf{C}_{Av}^{\sigma}\mathbf{X}_v + \sum_{j=1}^{5}\mathbf{C}_{A\alpha_j}^{\sigma} v_j = -\mathbf{C}_{A\alpha_{in}}^{\sigma} v_{in} - \mathbf{C}_{A\alpha_{out}}^{\sigma} v_{out}, \quad (13a)$$

$$\mathbf{C}_{Av}^{\sigma^T}\frac{d\mathbf{X}_A}{dt} + \mathbf{M}_{vv}^{\sigma}\mathbf{X}_v + \sum_{j=1}^{5}\mathbf{C}_{v\alpha_j}^{\sigma} v_j = -\mathbf{C}_{v\alpha_{in}}^{\sigma} v_{in} - \mathbf{C}_{v\alpha_{out}}^{\sigma} v_{out} \quad (13b)$$

with

$$[\mathbf{M}_{AA}^{\nu}]_{k,l} = \int_D \nu \mathbf{curl}\mathbf{w}_k^1 \cdot \mathbf{curl}\mathbf{w}_l^1 dD,$$
$$[\mathbf{N}_{AA}^{\sigma}]_{k,l} = \int_{D_c} \sigma \mathbf{w}_k^1 \cdot \mathbf{w}_l^1 dD_c,$$
$$[\mathbf{C}_{Av}^{\sigma}]_{k,l} = \int_{D_c} \sigma \mathbf{w}_k^1 \cdot \mathbf{grad}w_l^0 dD_c,$$
$$\left[\mathbf{C}_{A\alpha_j}^{\sigma}\right]_k = \int_{D_c} \sigma \mathbf{w}_k^1 \cdot \mathbf{grad}\alpha_j dD_c,$$
$$[\mathbf{M}_{vv}^{\sigma}]_{k,l} = \int_{D_c} \sigma \mathbf{grad}w_k^0 \cdot \mathbf{grad}w_l^0 dD_c,$$
$$\left[\mathbf{C}_{v\alpha_j}^{\sigma}\right]_k = \int_{D_c} \sigma \mathbf{grad}w_k^0 \cdot \mathbf{grad}\alpha_j dD_c$$

with $\mathbf{M}^T$ the transpose of the matrix $\mathbf{M}$. By supposing that the scalar product $\alpha_j \cdot \alpha_k$ is equal to 0 for $j \neq k$ with $j, k = \{in, out, 1, 2, 3, 4, 5\}$, the (9) associated with each current i_k becomes

$$\mathbf{C}_{A\alpha_k}^{\sigma^T}\frac{d\mathbf{X}_A}{dt} + \mathbf{C}_{v\alpha_k}^{\sigma^T}\mathbf{X}_v + M_{\alpha_k\alpha_k}^{\sigma} v_k - i_k = 0$$
$$\text{with } M_{\alpha_k\alpha_k}^{\sigma} = \int_{D_c} \sigma \mathbf{grad}\alpha_k \cdot \mathbf{grad}\alpha_k dD_c. \quad (14)$$

Algorithm 1: Pseudocode for CLN Algorithm.

Input: $\mathbf{K}, \mathbf{N}, \mathbf{F}, n$
Step 0: solve $\mathbf{K}\mathbf{x}_1 = \mathbf{F}$, set $\mathbf{u}_1 = \mathbf{x}_1$ and compute $L_1 = \mathbf{u}_1^T \mathbf{K} \mathbf{u}_1$
for $q = 1$ **to** n **do**
  Step 1: compute $\mathbf{v}_{2q} = \mathbf{v}_{2q-2} + \mathbf{u}_{2q-1} \frac{1}{L_{2q-1}}$
  Step 2: compute $\frac{1}{R_{2q}} = \mathbf{v}_{2q}^T \mathbf{N} \mathbf{v}_{2q}$
  Step 3: solve $\mathbf{K}\mathbf{x}_{2q+1} = \mathbf{N}\mathbf{v}_{2q} R_{2q}$
  Step 4: compute $\mathbf{u}_{2q+1} = \mathbf{u}_{2q-1} - \mathbf{x}_{2q+1}$
  Step 5: compute $L_{2q-1} = \mathbf{u}_{2q+1}^T \mathbf{K} \mathbf{u}_{2q+1}$
end for
Return: $\{\mathbf{u}_1, \cdots, \mathbf{u}_{2n+1}\}$, $\{\mathbf{v}_2, \cdots, \mathbf{v}_{2n}\}$, $\{L_1, \cdots, L_{2n+1}\}$, $\{R_2, \cdots, R_{2n}\}$

The equation of the electrical load is

$$R_c i_5 + L_c \frac{di_5}{dt} - v_5 + v_{out} = 0. \tag{15}$$

In order to obtain a numerical model of the PCB with transistors, the system of equations composed by (13), (14), and (15) is combined with models of the power switches.

IV. Equivalent Circuit Based on the CLN Approach

In the following, a procedure based on the CLN method is presented in order to extract an equivalent electrical circuit from a FE model. First, the case of a Single Input Single Output (SISO) is developed to introduce the CLN method. Then, the CLN approach is extended to the case of Multiple Inputs Multiple Outputs (MIMO). Finally, the equivalent CLN circuit of the PCB is developed.

A. Principle of SISO CLN Method

For simplicity, we will work in the frequency domain using the Laplace transformation and consider the following system of N equations with N DoF written in this form

$$\mathbf{K}\mathbf{X} + s\mathbf{N}\mathbf{X} = I(s)\mathbf{F}, \tag{16}$$

$$Y(s) = s\mathbf{F}^T\mathbf{X} \tag{17}$$

where $\mathbf{X}$ is the state vector of dimension N, $\mathbf{K} \in \mathbb{R}^{N\times N}$ and $\mathbf{N} \in \mathbb{R}^{N\times N}$ are symmetric matrices, $\mathbf{F}$ is a vector enabling to impose the source term $I(s) \in \mathbb{C}$, s is a complex variable, and $Y(s)$ is the quantity of interest. The CLN approach is based on the self-adjoint Lanczos method [8] where the Algorithm 1 is used to calculate the constants $\{L_1, \ldots, L_{2n+1}\}$ and $\{R_2, \ldots, R_{2n}\}$ as well as the reduced bases $\mathbf{U}_n$ and $\mathbf{V}_n$ defined by

$$\mathbf{U}_n = [\mathbf{u}_1\, \mathbf{u}_3\, \cdots\, \mathbf{u}_{2q-1}\, \cdots\, \mathbf{u}_{2n-1}], \tag{18}$$

$$\mathbf{V}_n = [\mathbf{v}_2\, \mathbf{v}_4\, \cdots\, \mathbf{v}_{2q}\, \cdots\, \mathbf{v}_{2n}]. \tag{19}$$

The bases $\mathbf{U}_n \in \mathbb{R}^{N\times n}$ and $\mathbf{V}_n \in \mathbb{R}^{N\times n}$ span the same space. In the CLN method, we seek for an approximation $\mathbf{X}'$ of $\mathbf{X}$ in

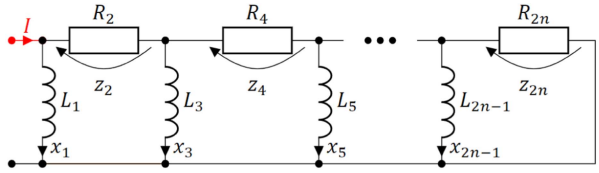

Fig. 5. Equivalent CLN electrical circuit for SISO.

the space spanned by reduced basis $\mathbf{U}_n$ or $\mathbf{V}_n$ such that

$$\mathbf{X} \approx \mathbf{X}' = \sum_{q=1}^{n} \mathbf{u}_{2q-1} x_{2q-1}, \tag{20}$$

$$s\mathbf{X} \approx s\mathbf{X}' = \sum_{q=1}^{n} \mathbf{v}_{2q} z_{2q} \tag{21}$$

where $x_1, \ldots, x_{2n-1}$ and $z_2, \ldots, z_{2n}$ are the coefficients to be determined. Then, the number of unknowns of the problem is not related to the size of the full system N but to the size of the reduced basis n, which can be chosen much smaller than N. To derive the relationship between these coefficients $x_1, \ldots, x_{2n-1}$ and $z_2, \ldots, z_{2n}$, $\mathbf{X}$ and $s\mathbf{X}$ are replaced by their expressions (20) and (21) in (16) and a Galerkin projection is performed using the reduced basis $\mathbf{U}_n$ in order to obtain the equation system to be solved

$$\mathbf{U}_n^T\mathbf{K}\sum_{q=1}^{n} \mathbf{u}_{2q-1} x_{2q-1} + \mathbf{U}_n^T\mathbf{N}\sum_{q=1}^{n} \mathbf{v}_{2q} z_{2q} = I(s)\mathbf{U}_n^T\mathbf{F}. \tag{22}$$

Applying properties of the vectors from bases $\mathbf{U}_n$ or $\mathbf{V}_n$, we can derive the following relationships for the coefficients from (22):

$$x_1 + \tfrac{1}{R_2} z_2 = I(s), \tag{23}$$

$$\forall q \in [2, n] \quad x_{2q-1} + \left(\tfrac{1}{R_{2q}} z_{2q} - \tfrac{1}{R_{2q-2}} z_{2q-2}\right) = 0,$$

$$z_{2n} = sL_{2n-1}x_{2n-1},$$

$$\forall q \in [1, n-1] \quad z_{2q} = s(L_{2q-1}x_{2q-1} - L_{2q+1}x_{2q+1}). \tag{24}$$

The previous equation system can be interpreted as the equation system of an equivalent electrical circuit composed of n stages, similar to the one depicted in Fig. 5 where the source term $I(s)$ of (16) is the input current, the coefficients $\{L_1, \cdots, L_{2n+1}\}$ and $\{R_2, \cdots, R_{2n}\}$ determined by the algorithm (1) are the values of the inductances and resistors, respectively, the coefficients to be computed $x_1, \ldots, x_{2n-1}$ and $z_2, \ldots, z_{2n}$ are, respectively, the currents associated with the inductances and the voltages at the terminals of the resistors. To summarize, the CLN method consists in applying the algorithm (1) to the equation system (16) to define the parameters of the equivalent CLN electrical circuit (Fig. 5). In terms of numerical technic used to solve matrix systems, an iterative approach based on a preconditioned conjugate gradient technic which is well adapted for matrix systems obtained from the FE method has been applied. Then, the currents and voltages can be computed by solving the equivalent CLN circuit in the frequency or time domain enabling

to reconstruct an approximation given by (20) or (21) of the solution $\mathbf{X}$ of the equation system (16).

B. MIMO CLN Method

If the system has $\mathcal{M}$ source terms $i_{0,1}(s), i_{0,2}(s), \ldots, i_{0,\mathcal{M}}(s)$, (16) is modified as

$$\mathbf{KX} + s\mathbf{NX} = \sum_{m=1,\mathcal{M}} i_{0,m}(s)\mathbf{F}_m, \tag{25}$$

$$\forall m \in [1, \mathcal{M}] \quad Y_m(s) = s\mathbf{F}_m^T\mathbf{X} \tag{26}$$

with $\mathbf{F}_m$ a vector associated with the source $i_{0,m}(s)$ and $Y_1(s), Y_2(s), \ldots, Y_{\mathcal{M}}(s)$ the quantities of interest. We define the matrix $\mathbf{F} \in \mathbb{R}^{N\times\mathcal{M}}$ by

$$\mathbf{F} = [\mathbf{F}_1 \quad \mathbf{F}_2 \quad \cdots \quad \mathbf{F}_{\mathcal{M}}] \tag{27}$$

$\mathbf{I}_{\mathcal{M}} \in \mathbb{R}^{\mathcal{M}\times 1}$ the source vector and $\mathbf{Y}_{\mathcal{M}} \in \mathbb{R}^{\mathcal{M}\times 1}$ the vector of the quantities of interest such that

$$\mathbf{I}_{\mathcal{M}} = [i_{0,1}(s) \quad i_{0,2}(s) \quad \cdots \quad i_{0,\mathcal{M}}(s)]^T, \tag{28}$$

$$\mathbf{Y}_{\mathcal{M}} = [Y_1(s) \quad Y_2(s) \quad \cdots \quad Y_{\mathcal{M}}(s)]^T. \tag{29}$$

Then, the equation system (25) is rewritten as follows:

$$\mathbf{KX} + s\mathbf{NX} = \mathbf{FI}_{\mathcal{M}}. \tag{30}$$

The MIMO algorithm 2 is an extension of the SISO self adjoint Lanczos algorithm (1). It is applicable to matrix systems under the form of (30), provided that $\mathbf{K}$ and $\mathbf{N}$ are real symmetric matrices and $\mathbf{F}$ is a real matrix. Compared to the SISO algorithm, the MIMO algorithm gives a set of matrices $\{\mathbf{u}_1, \ldots, \mathbf{u}_{2n+1}\}$ and $\{\mathbf{v}_2, \ldots, \mathbf{v}_{2n}\}$ rather than a set of vectors such that

$$\forall\, i \in [1, n]\, \mathbf{u}_{2i-1} \in \mathbb{R}^{N\times\mathcal{M}} \quad \text{and} \quad \mathbf{v}_{2i} \in \mathbb{R}^{N\times\mathcal{M}}. \tag{31}$$

The reduced basis $\mathbf{U}_n$ is obtained by concatenating the set of matrices $\{\mathbf{u}_1, \ldots, \mathbf{u}_{2n+1}\}$.

$$\mathbf{U}_n = \begin{bmatrix}\mathbf{u}_1 & \mathbf{u}_3 & \cdots & \mathbf{u}_{2n-1}\end{bmatrix} \in \mathbb{R}^{N\times(\mathcal{M}\cdot n)} \tag{32}$$

where the brackets in (32) indicate horizontal concatenation, e.g.,

$$\begin{bmatrix}\mathbf{u}_1 & \mathbf{u}_3\end{bmatrix} = [\mathbf{u}_{1,1}\, \mathbf{u}_{1,2} \cdots \mathbf{u}_{1,\mathcal{M}}\, \mathbf{u}_{3,1}\, \mathbf{u}_{3,2} \cdots \mathbf{u}_{3,\mathcal{M}}] \tag{33}$$

with $\mathbf{u}_{1,i}$ and $\mathbf{u}_{3,i}$ the vectors of the ith column of the matrices $\mathbf{u}_1$ and $\mathbf{u}_3$, respectively. Then, the reduced basis $\mathbf{U}_n$ is composed of $\mathcal{M}\cdot n$ columns. Similarly, the reduced basis $\mathbf{V}_n$ is defined by

$$\mathbf{V}_n = \begin{bmatrix}\mathbf{v}_2 & \mathbf{v}_4 & \cdots & \mathbf{v}_{2n}\end{bmatrix} \in \mathbb{R}^{N\times(\mathcal{M}\cdot n)}. \tag{34}$$

At the same time, the MIMO self adjoint Lanczos algorithm gives a set of symmetric matrices $\{\mathbf{L}_1, \ldots, \mathbf{L}_{2n+1}\}$ and $\{\mathbf{R}_2, \ldots, \mathbf{R}_{2n}\}$

$$\forall q \in [1, n-1], \quad \mathbf{L}_{2q-1} \in \mathbb{R}^{\mathcal{M}\times\mathcal{M}} \tag{35}$$

$$\forall q \in [2, n], \quad \mathbf{R}_{2q} \in \mathbb{R}^{\mathcal{M}\times\mathcal{M}}. \tag{36}$$

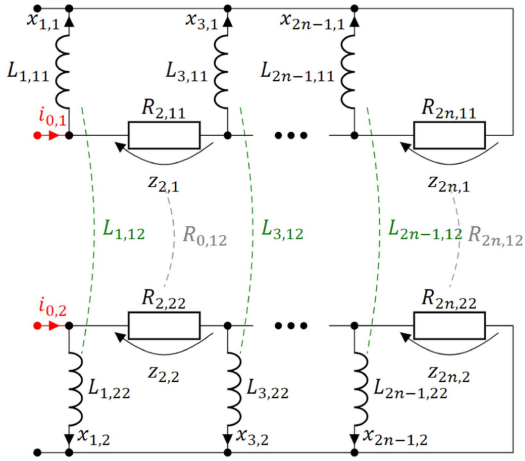

Fig. 6. Equivalent CLN electrical circuit for MIMO.

Algorithm 2: Pseudocode for MIMO CLN Algorithm.

Input: $\mathbf{K}, \mathbf{N}, \mathbf{F}, n$
Step 0: solve $\mathbf{Kx}_1 = \mathbf{F}$, set $\mathbf{u}_1 = \mathbf{x}_1$ and compute $\mathbf{L}_1 = \mathbf{u}_1^T\mathbf{Ku}_1$
for $q = 1$ **to** n **do**
  Step 1: compute $\mathbf{v}_{2q} = \mathbf{v}_{2q-2} + \mathbf{u}_{2q-1}\mathbf{L}_{2q-1}^{-1}$
  Step 2: compute $\mathbf{R}_{2q}^{-1} = \mathbf{v}_{2q}^T\mathbf{Nv}_{2q}$
  Step 3: solve $\mathbf{Kx}_{2q+1} = \mathbf{Nv}_{2q}\mathbf{R}_{2q}$
  Step 4: compute $\mathbf{u}_{2q+1} = \mathbf{u}_{2q-1} - \mathbf{x}_{2q+1}$
  Step 5: compute $\mathbf{L}_{2q+1} = \mathbf{u}_{2q+1}^T\mathbf{Ku}_{2q+1}$
end for
Return: $\{\mathbf{u}_1, \ldots, \mathbf{u}_{2n+1}\}$, $\{\mathbf{v}_2, \ldots, \mathbf{v}_{2n}\}$, $\{\mathbf{L}_1, \ldots, \mathbf{L}_{2n+1}\}$, $\{\mathbf{R}_2, \ldots, \mathbf{R}_{2n}\}$

An approximation $\mathbf{X}'$ of $\mathbf{X}$ in the space spanned by reduced basis $\mathbf{U}_n$ or $\mathbf{V}_n$ can be obtained by the following expression:

$$\mathbf{X} \approx \mathbf{X}' = \sum_{q=1}^{n} \mathbf{u}_{2q-1}\mathbf{x}_{2q-1},$$

$$s\mathbf{X} \approx s\mathbf{X}' = \sum_{q=1}^{n} \mathbf{v}_{2q}\mathbf{z}_{2q} \tag{37}$$

where $\mathbf{x}_1 \in \mathbb{R}^{\mathcal{M}\times 1}, \ldots, \mathbf{x}_{2n-1} \in \mathbb{R}^{\mathcal{M}\times 1}$ and $\mathbf{z}_2 \in \mathbb{R}^{\mathcal{M}\times 1}$, $\ldots, \mathbf{z}_{2n} \in \mathbb{R}^{\mathcal{M}\times 1}$ are vectors to be determined. Then, the number of unknowns of the problem is not related to the size of the full system N but to the size of the reduced basis $n\cdot\mathcal{M}$, which can be chosen much smaller than N. Applying a similar development for the MIMO case than for the SISO, we can prove that the vectors $\mathbf{x}_1 \in \mathbb{R}^{\mathcal{M}\times 1}, \ldots, \mathbf{x}_{2n-1} \in \mathbb{R}^{\mathcal{M}\times 1}$ and $\mathbf{z}_2 \in \mathbb{R}^{\mathcal{M}\times 1}, \ldots, \mathbf{z}_{2n} \in \mathbb{R}^{\mathcal{M}\times 1}$ defined in (37) verify the equations

$$\mathbf{x}_1 + \mathbf{R}_2^{-1}\mathbf{z}_2 = \mathbf{I}_{\mathcal{M}}, \tag{38}$$

$$\forall q \in [2, n] \quad \mathbf{x}_{2q-1} + (\mathbf{R}_{2q}^{-1}\mathbf{z}_{2q} - \mathbf{R}_{2q-2}^{-1}\mathbf{z}_{2q-2}) = 0,$$

$$\mathbf{z}_{2n} = s\mathbf{L}_{2n-1}\mathbf{x}_{2n-1},$$

$$\forall q \in [1, n-1] \quad \mathbf{z}_{2q} = s(\mathbf{L}_{2q-1}\mathbf{x}_{2q-1} - \mathbf{L}_{2q+1}\mathbf{x}_{2q+1}). \tag{39}$$

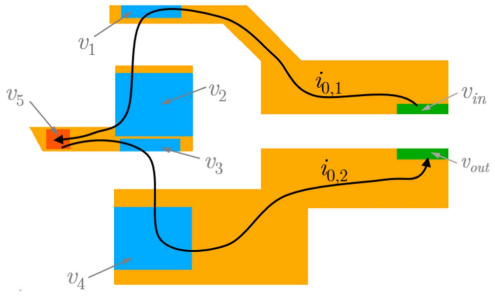

Fig. 7. Definition of the branch currents $i_{0,1}$ and $i_{0,2}$.

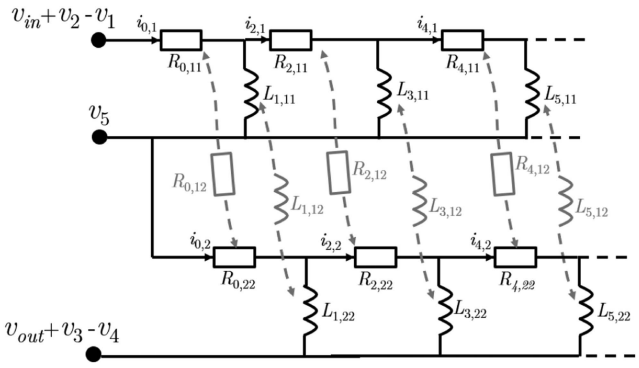

Fig. 8. Equivalent CLN circuit of the PCB.

It can be shown that these equations verify by the entries of the vectors $\mathbf{x}_1 \in \mathbb{R}^{\mathcal{M}\times 1}, \ldots, \mathbf{x}_{2n-1} \in \mathbb{R}^{\mathcal{M}\times 1}$ and $\mathbf{z}_2 \in \mathbb{R}^{\mathcal{M}\times 1}, \ldots, \mathbf{z}_{2n} \in \mathbb{R}^{\mathcal{M}\times 1}$ are in fact the equations of an equivalent electrical circuit with $\mathcal{M}$ inputs and n stages. The values of the self and mutual inductances as well as those of the resistors of an equivalent electrical circuit are given by the values of the matrices $\{\mathbf{L}_1, \ldots, \mathbf{L}_{2n+1}\}$ and $\{\mathbf{R}_2, \ldots, \mathbf{R}_{2n}\}$. An equivalent CLN circuit in the case of $\mathcal{M} = 2$ is given by Fig. 6.

C. Application to the PCB

The MQS FE model associated with the PCB, as described in Section III-B, is now considered. To apply the CLN approach, an equation system based on (13) and (14) is defined such that

$$\begin{bmatrix} \mathbf{M}^{\nu}_{AA} & \mathbf{C}^{\sigma}_{Av} & \mathbf{C}^{\sigma}_{A\alpha} \\ 0 & \mathbf{M}^{\sigma}_{vv} & \mathbf{C}^{\sigma}_{v\alpha} \\ 0 & \mathbf{C}^{\sigma T}_{v\alpha} & \mathbf{M}^{\sigma}_{\alpha\alpha} \end{bmatrix} \begin{bmatrix} \mathbf{X}_A \\ \mathbf{X}_v \\ \mathbf{X}_V \end{bmatrix} + \begin{bmatrix} \mathbf{M}^{\sigma}_{AA} & 0 & 0 \\ \mathbf{C}^{\sigma T}_{Av} & 0 & 0 \\ \mathbf{C}^{\sigma T}_{A\alpha} & 0 & 0 \end{bmatrix} \frac{d}{dt} \begin{bmatrix} \mathbf{X}_A \\ \mathbf{X}_v \\ \mathbf{X}_V \end{bmatrix} = \begin{bmatrix} 0 \\ 0 \\ \mathbf{J} \end{bmatrix} \tag{40}$$

with $\mathbf{X}_V$ the vector of the scalar potentials v_j and $\mathbf{J}$ the vector of the currents i_j such that $\mathbf{X}_V = [v_{in}\, v_{out}\, v_1\, v_2\, v_3\, v_4\, v_5]^T$ and $\mathbf{J} = [i_{in}\, i_{out}\, i_1\, i_2\, i_3\, i_4\, i_5]^T$, respectively, $\mathbf{C}^{\sigma}_{A\alpha}$ and $\mathbf{C}^{\sigma}_{v\alpha}$ matrices defined by $\mathbf{C}^{\sigma}_{A\alpha} = [\mathbf{C}^{\sigma}_{A\alpha_{in}}\, \mathbf{C}^{\sigma}_{A\alpha_{out}}\, \mathbf{C}^{\sigma}_{A\alpha_1}\, \mathbf{C}^{\sigma}_{A\alpha_2}\, \mathbf{C}^{\sigma}_{A\alpha_3}\, \mathbf{C}^{\sigma}_{A\alpha_4}\, \mathbf{C}^{\sigma}_{A\alpha_5}]$ and $\mathbf{C}^{\sigma}_{v\alpha} = [\mathbf{C}^{\sigma}_{v\alpha_{in}}\, \mathbf{C}^{\sigma}_{v\alpha_{out}}\, \mathbf{C}^{\sigma}_{v\alpha_{i1}}\, \mathbf{C}^{\sigma}_{v\alpha_2}\, \mathbf{C}^{\sigma}_{v\alpha_3}\, \mathbf{C}^{\sigma}_{v\alpha_4}\, \mathbf{C}^{\sigma}_{v\alpha_5}]$, respectively, and $\mathbf{M}^{\sigma}_{\alpha\alpha}$ a diagonal matrix defined by $[\mathbf{M}^{\sigma}_{\alpha\alpha}]_{k,k} = M^{\sigma}_{\alpha_k\alpha_k}$. Based on the studied PCB, two branch currents $i_{0,1}$ and $i_{0,2}$ are introduced and illustrated in Fig. 7. Then, the current vector $\mathbf{J}$ can be expressed by

$$\begin{aligned} \mathbf{J} &= i_{0,1} \begin{bmatrix} 1 & 0 & -1 & 1 & 0 & 0 & -1 \end{bmatrix}^T \\ &\quad + i_{0,2} \begin{bmatrix} 0 & -1 & 0 & 0 & -1 & 1 & 1 \end{bmatrix}^T \\ &= i_{0,1}\mathbf{b}_1 + i_{0,2}\mathbf{b}_2. \end{aligned} \tag{41}$$

The equation system (40) differs from the one presented in (30) for the MIMO case. The matrices of this system are not symmetric. Consequently, the CLN method presented above can not be applied directly. To perform the CLN approach, an alternative equation system is defined with only the vector $\mathbf{X}_A$ as solution. Based on (40), the vectors $\mathbf{X}_v$ and $\mathbf{X}_V$ are expressed as function of $\mathbf{X}_A$. An equivalent equation system to (25) is determined with

$$\mathbf{K} = \mathbf{M}^{\nu}_{AA},$$

$$\mathbf{N} = \mathbf{M}^{\sigma}_{AA} - \begin{bmatrix} \mathbf{C}^{\sigma}_{Av} \mathbf{C}^{\sigma}_{A\alpha} \end{bmatrix} \begin{bmatrix} \mathbf{M}^{\sigma}_{vv} & \mathbf{C}^{\sigma}_{v\alpha} \\ \mathbf{C}^{\sigma T}_{v\alpha} & \mathbf{M}^{\sigma}_{\alpha\alpha} \end{bmatrix}^{-1} \begin{bmatrix} \mathbf{C}^{\sigma T}_{Av} \\ \mathbf{C}^{\sigma T}_{A\alpha} \end{bmatrix},$$

$$\mathbf{FI}_{\mathcal{M}} = \begin{bmatrix} \mathbf{C}^{\sigma}_{Av} \mathbf{C}^{\sigma}_{A\alpha} \end{bmatrix} \begin{bmatrix} \mathbf{M}^{\sigma}_{vv} & \mathbf{C}^{\sigma}_{v\alpha} \\ \mathbf{C}^{\sigma T}_{v\alpha} & \mathbf{M}^{\sigma}_{\alpha\alpha} \end{bmatrix}^{-1} \begin{bmatrix} 0 \\ \mathbf{J} \end{bmatrix},$$

with $\mathbf{J} = \mathbf{b}_1 i_{0,1} + \mathbf{b}_2 i_{0,2}$ and $\mathbf{X} = \mathbf{X}_A$.

Then, the CLN approach with $\mathcal{M} = 2$ is implemented. To account for the dc resistive effect of the PCB, an initial step $n = 0$ consists to solve two electrokinetic problems, one for each current $i_{0,1}$ and $i_{0,2}$ equal to 1A. Then, we solve

$$\begin{bmatrix} \mathbf{M}^{\sigma}_{vv} & \mathbf{C}^{\sigma}_{v\alpha} \\ \mathbf{C}^{\sigma T}_{v\alpha} & \mathbf{M}^{\sigma}_{\alpha\alpha} \end{bmatrix} \begin{bmatrix} \mathbf{X}^{j}_{v,0} \\ \mathbf{X}^{j}_{V,0} \end{bmatrix} = \begin{bmatrix} 0 \\ \mathbf{b}_j \end{bmatrix} \text{ with } j = \{1, 2\}. \tag{42}$$

The dc resistor matrix $\mathbf{R}_0$ of size 2×2 is defined by

$$\mathbf{R}_0 = \begin{bmatrix} \mathbf{b}_1 & \mathbf{b}_2 \end{bmatrix}^T \begin{bmatrix} \mathbf{X}^1_{V,0} & \mathbf{X}^2_{V,0} \end{bmatrix}. \tag{43}$$

Finally, the equivalent CLN circuit associated with the PCB is given by Fig. 8.

The voltages associated with the equivalent CLN circuit are expressed by

$$\begin{bmatrix} v_{in} + v_2 - v_1 - v_5 \\ v_5 + v_4 - v_3 - v_{out} \end{bmatrix} = \mathbf{R}_0 \begin{bmatrix} i_{0,1} \\ i_{0,2} \end{bmatrix} + s\mathbf{L}_1 \begin{bmatrix} x_{1,1} \\ x_{1,2} \end{bmatrix} \tag{44}$$

and the current i_5 by

$$i_5 = i_{0,1} - i_{0,2}. \tag{45}$$

V. Validation of the Equivalent CLN Circuit

In order to valid the equivalent CLN circuit of the PCB, an academic example is considered. The transistors K_1 and K_2 are replaced by ideal switches modeled by resistors R_{K_1} and R_{K_2} which can take two fixed values R_{on} or R_{off} (Fig. 9). When a switch is closed the resistor is R_{on} otherwise R_{off} with a small

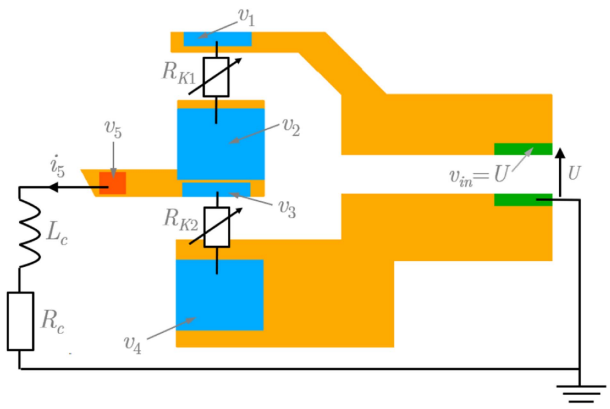

Fig. 9. PCB with the electrical load and ideal switches.

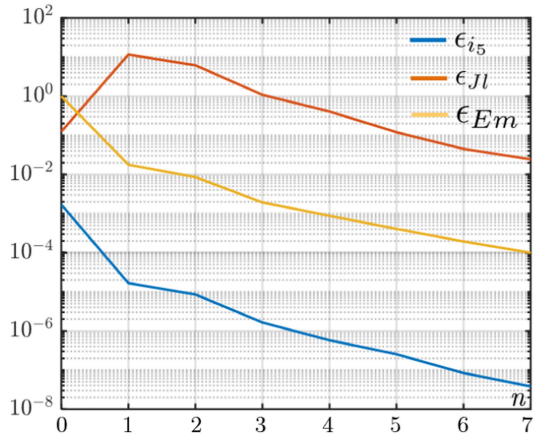

Fig. 10. Relative errors versus the stages number n on i_5, Jl of the PCB and Em.

value for R_{on} and a high value for R_{off}. Then, we consider

$$t \in [0; T/2] : R_{K_1} = R_{on} \text{ and } R_{K_2} = R_{off}, \quad (46)$$

$$t \in [T/2; T] : R_{K_1} = R_{off} \text{ and } R_{K_2} = R_{on} \quad (47)$$

where T is the time period ($T = 1/f$). Fig. 10 presents the PCB connected to the electrical load and to ideal switches. The equations introduced by the resistors R_{K_1} and R_{K_2} are

$$v_1 - v_2 = R_{K_1} i_1 \quad (48a)$$

$$v_3 - v_4 = R_{K_2} i_3 \quad (48b)$$

$$i_1 = -i_2 \text{ and } i_3 = -i_4. \quad (48c)$$

The full model of the studied example is based on the FE model defined by (13) and (14) combined with (15) and (48). The reduced model is based on (44), (45) and Fig. 8 associated with (15) and (48). The results obtained from the reduced model are compared with those from the full model. The time step is fixed to 50 ns and the number of time steps is 140. Figure (49) presents the relative error versus the stages number n of the equivalent CLN circuit on the current i_5, the Joule losses Jl of the PCB and the magnetic energy Em of the entire domain associated with the reduced model (denoted RM), with reference

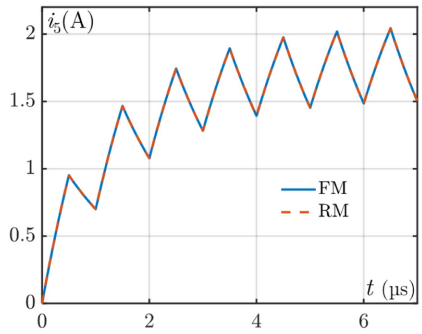

Fig. 11. Waveform of the current i_5 versus the time obtained from the full and reduced models.

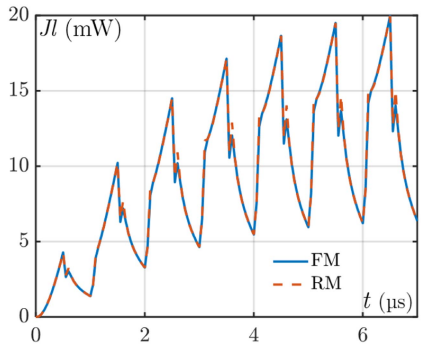

Fig. 12. Waveform of the Joule losses versus the time obtained from the full and reduced models.

to the results from the full model (denoted FM), computed by

$$\epsilon_V = \frac{||\mathbf{V}_{FM} - \mathbf{V}_{RM}||_2}{||\mathbf{V}_{FM}||_2} \quad (49)$$

with $||\cdot||_2$ the $\mathbf{L}_2$ norm and $\mathbf{V}$ the value vector of i_5, Jl or Em for all time steps. With a small number of stages for the equivalent CLN circuit, the accuracy of the reduced model is sufficient for the current i_5 and the magnetic energy Em. In order to obtain an acceptable error for the Joule losses, the number of stages must be increased. In fact, this interest quantity depends on the expression of the electrical field in the PCB which is a function of the derivative of the magnetic vector potential and of the electric scalar potential (6). In the following, we consider the equivalent CLN circuit with $n = 7$ stages. Figs. 11–13 present the waveforms of the current i_5, Joule losses Jl, and magnetic energy Em versus the time obtained from the full and reduced models.

For all global interest quantities, the waveforms given by the reduced model show good agreement with those from the full model. Figs. 14 and 16 present the distributions of the current density at the beginning of the simulation ($t = 1.05\,\mu$s) and at $t = 4.5\,\mu$s. For the first time instant, the current flows though the top conductive track of the PCB and for the second time instant, it flows though the bottom conductive track. Figs. 15 and 17 present the distributions of the current density error for the same time instants. For both time instants, the skin effect can be observed and the magnitude of the errors is small compared

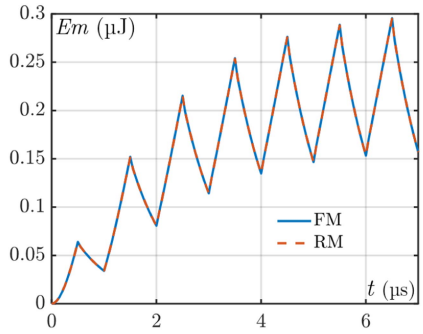

Fig. 13. Waveform of the magnetic energy versus the time obtained from the full and reduced models.

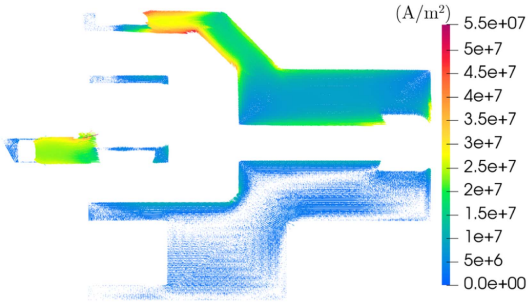

Fig. 14. Distribution of the current density obtained from the reduced model at $t = 1.05\ \mu$s.

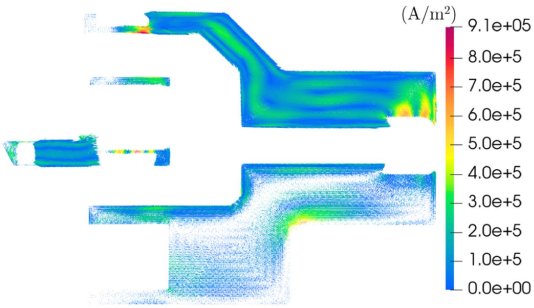

Fig. 15. Distribution of the error on the current density at $t = 1.05\ \mu$s.

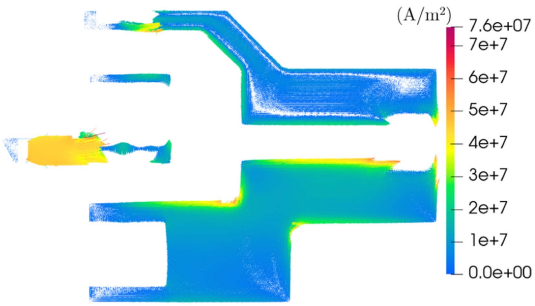

Fig. 16. Distribution of the current density obtained from the reduced model at $t = 4.5\ \mu$s.

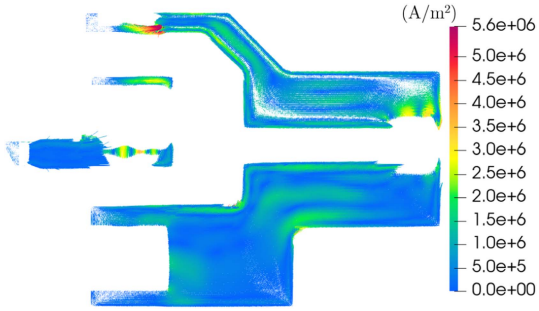

Fig. 17. Distribution of the error on the current density at $t = 4.5\ \mu$s.

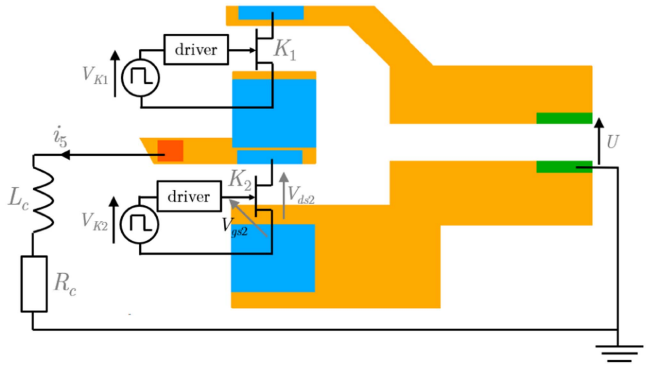

Fig. 18. Simulation scheme of the PCB with the electrical load and GaN transistors.

with this one of the current density. For the second time instant, a current flows through from $\Gamma_{E,1}$ to $\Gamma_{E,in}$ during a short transient state where the electric potential v_1 becomes higher than v_{in} due to the opening of K_1 . In terms of computational time, the determination of the equivalent CLN circuit requires 10 min. For all time steps, the computational time to solve the full model is about 60 min and 1 s for the reduced model. For both models, the time of the postprocessing requires to calculate the global and local quantities such that the Joule losses or the magnetic energy and the distribution of the current density is 10 min.

VI. Co-Simulation

Based on the system presented in Fig. 1 and described in [12] (photographs of the prototype and experimental setup), a co-simulation is done (Fig. 18). The equivalent CLN circuit of the PCB is combined with models of GaN transistors K_1 and K_2. The model of GaN transistors is based on SPICE models of transistors GS66520B provided by the manufacturer [15]. In a first part, the influence of PCB inductive effect is studied and in the second part, the results obtained from the co-simulation are compared with the measurements. For all co-simulations, the time step is fixed to 0.1 ns and the simulation time is 7 μs (seven switching periods).

A. Study of the PCB Inductive Effect Influence

To investigate the influence of the PCB inductive effect, two co-simulations are considered. For the first one, the stage number

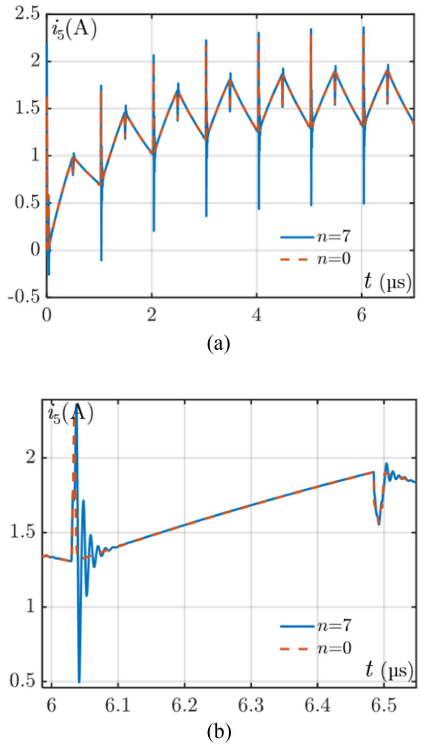

Fig. 19. Waveform of the current i_5 for $n = 0$ and 7.

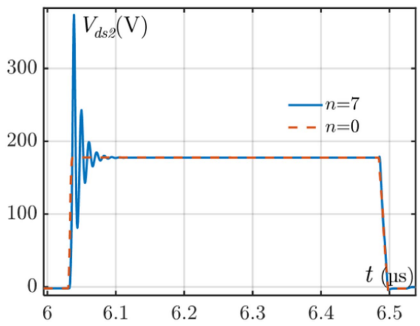

Fig. 20. Waveform of the drain-source voltage V_{ds2} associated with the transistor K_2 for $n = 0$ and 7.

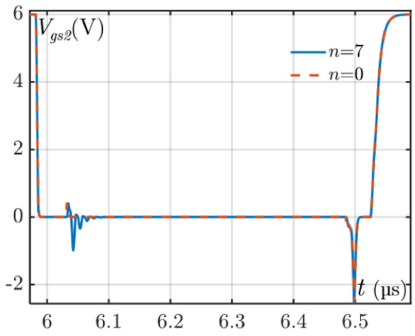

Fig. 21. Waveform of the gate-source voltage V_{gs2} associated with the transistor K_2 for $n = 0$ and 7.

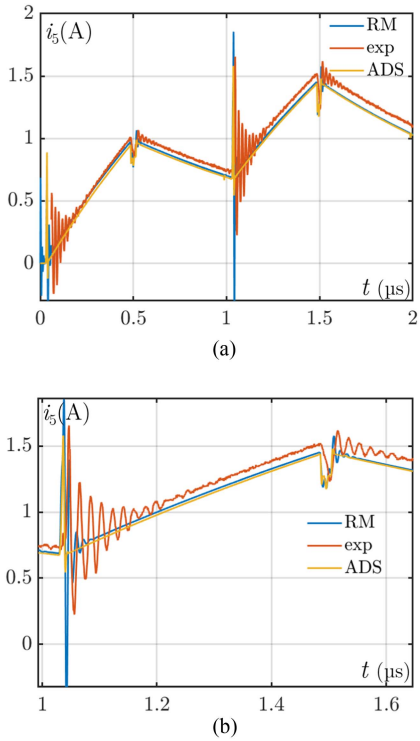

Fig. 22. Waveform of the current i_5 obtained from the co-simulation (RM), measures (exp.) and ADS software.

n is fixed to 0, the equivalent CLN circuit is composed by the resistor matrix $\mathbf{R}_0$ which takes only into account the DC resistive effect of the PCB. For the second co-simulation, the resistive and inductive effects are taken into account with $n = 7$. For $n = 0$ and 7, Figs. 19–21 present the waveform of the current i_5, the drain-source voltage V_{ds2}, and the gate-source voltage V_{gs2}. The influence of the PCB inductive effect can be clearly observed. Indeed, supplementary oscillations are introduced for each electrical quantity due to the stray inductances and parasitic capacitances of system.

B. Comparison With Measurements

The results obtained from the co-simulation considering $n = 7$ stages for the equivalent CLN circuit associated with the reduced model (denoted by RM) are compared with the measurements (denoted by exp.) and with results from Advanced Design System (ADS) software. Figs. 22–24 present the waveforms of the current i_5, the drain-source voltage V_{ds2} and the gate-source voltage V_{gs2} obtained from the co-simulation and from the measurements.

For each electrical quantity of interest, the waveform from the co-simulation deduced from the proposed approach is close to the measurement and also to the one obtained from ADS software which confirms the effectiveness of the developed approach. However, the high frequency ringings appearing after each switching are different. The frequency is about 51 MHz experimentally and 86 MHz by the co-simulation. This difference can be explained by the fact that this frequency depends on the

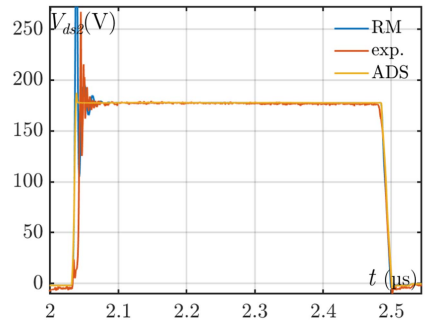

Fig. 23. Waveform of the drain-source voltage V_{ds2} obtained from the co-simulation (RM), measures (exp.) and ADS software.

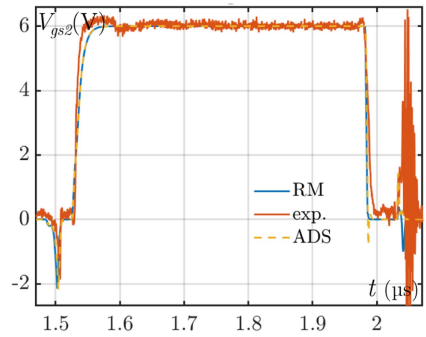

Fig. 24. Waveform of the gate-source voltage V_{gs2} obtained from the co-simulation (RM), measures (exp.) and ADS software.

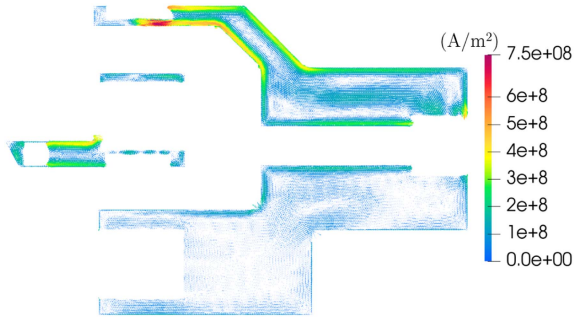

Fig. 25. Distribution of the current density at $t = 6.05$ μs.

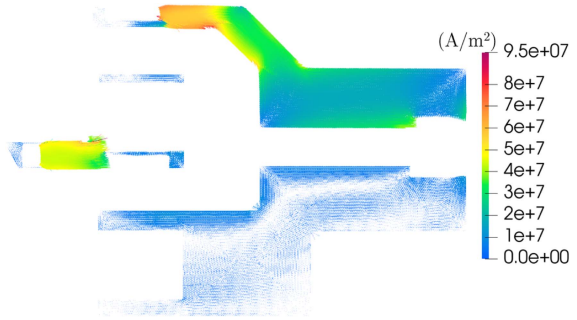

Fig. 26. Distribution of the current density at $t = 6.45$ μs.

inductance value associated with the PCB layout and interconnects from the dc bus to PCB and from PCB to the electrical load. From a modeling aspect, this value depends on the positioning and the length of the cables in the studied domain which does not exactly correspond to the experimental setup. The value of the inductance relies on the distribution of the magnetic flux density in the air surrounding the PCB. Then, the accuracy of this value depends also on the mesh quality of the air. A fine mesh leads to an accurate value but a huge computational time. However, the PCB layout of interconnects between boards, as well as the voltage and current probes behaviour (see [12]) are not taken into account in the proposed model. These model assumptions could be a possible explanation of the differences of the ringing in co-simulation results from the proposed approach and ADS software with the measurements. Then, these assumptions lead to also different values for the overvoltage on the waveform of voltage V_{ds2} about 265 V and 375 V obtained experimentally and by the proposed approach, respectively (Fig. 23). During the running of the co-simulation, the intermediate electrical quantities (currents and voltages) associated with the equivalent CLN circuit are stored. Then, based on these quantities and the reduced bases $\mathbf{U}_n$ and $\mathbf{V}_n$ defined by the CLN approach, the distribution of the current density can be defined for any time step. Figs. 25 and 26 present the distribution of the current density for $t = 6.05$ μs and 6.45 μs when K_1 is turned ON. For $t = 6.05$ μs, the skin effect can be observed on the distribution of current density. In fact, this time step is close to turn ON of the transistor K_1 where high frequency oscillations of the current appear (see Fig. 19(b). For $t = 6.45$ μs, the distribution of current density is mainly influenced by the geometry of the PCB. In terms of computational time, the co-simulation requires 80 s.

VII. Conclusion

The CLN approach has been performed to a MQS FE model associated with a PCB to derive an equivalent circuit. Then, the equivalent CLN circuit has been combined with GaN transistor models to define a co-simulation based on a half-bridge converter. This co-simulation has been used to study the inductive effect of the PCB on the electrical quantities. The results of the co-simulation were compared with measurements and showed good agreement. Additionally, the co-simulation is solved with an acceptable time (80 s for 70 k time steps), making the proposed approach suitable for use during the design phase of power converters. For a fixed geometry of the PCB, a parametric study could be easily done for different type of power switches on the evolution of global electrical quantities and current density distributions. For a fixed power switches, the electrical conductivity of the PCB and variations of its geometry could be considered as parameters of the problem in order to study their influences on global quantities and current density distributions. The PCB shape can be optimized in order to avoid hot spots and regions where the current density is small.

In terms of restriction, if the capacitive effect of a PCB cannot be neglected, the MQS problem is not adapted, e.g., in the case of a doubled-sided PCB or (insulated metal substrate) PCB.

Then, Darwin model could be considered [7]. Nevertheless, the determination of an equivalent electrical circuit from a FE model is still an open issue. This subject will be investigated by the authors in the future works.

REFERENCES

[1] G. Antonini, A. E. Ruehli, D. Romano, and F. Loreto, "The partial elements equivalent circuit method: The state of the art," *IEEE Trans. Electromagn. Compat.*, vol. 65, no. 6, pp. 1695–1714, Dec. 2023.

[2] J. He, S. Tao, and H. Wu, "A PEEC-based concise broadband physical circuit modeling method with parameter extraction for PCB inductive components," *IEEE Trans. Power Electron.*, vol. 35, no. 10, pp. 10852–10862, Oct. 2020.

[3] R. Torchio, F. Lucchini, J.-L. Schanen, O. Chadebec, and G. Meunier, "FFT-PEEC: A fast tool from CAD to power electronics simulations," *IEEE Trans. Power Electron.*, vol. 37, no. 1, pp. 700–713, Jan. 2022.

[4] R. Torchio, D. Voltolina, P. Bettini, F. Moro, and P. Alotto, "Marching on-in-time unstructured PEEC method for electrically large structures with conductive, dielectric, and magnetic media," *Electronics*, vol. 9, no. 2, pp. 1–17, 2020.

[5] J. Stysch, A. Klaedtke, and H. de Gersem, "Finite element extraction of frequency-dependent parasitics," *IEEE Trans. Magn.*, vol. 58, no. 9, Sep. 2022, Art. no. 7401104.

[6] Z. Ren, "Degenerated Whitney prism elements-general nodal and edge shell elements for field computation in thin structures," *IEEE Trans. Magn.*, vol. 34, no. 5, pp. 2547–2550, Sep. 1998.

[7] H. Taha, T. Henneron, Z. Tang, Y. Le Menach, L. Pace, and J.-P. Ducreux, "Electromagnetic modeling of PCB based on Darwin's model combined with degenerated prism whitney elements," *IEEE Trans. Power Electron.*, vol. 38, no. 1, pp. 678–691, Jan. 2023.

[8] A. Kameari, H. Ebrahimi, K. Sugahara, Y. Shindo, and T. Matsuo, "Cauer ladder network representation of eddy-current fields for model order reduction using finite-element method," *IEEE Trans. Magn.*, vol. 54, no. 3, Mar. 2018, Art. no. 7201804.

[9] S. Hiruma and H. Igarashi, "Model order reduction for linear time-invariant system with symmetric positive-definite matrices: Synthesis of Cauer-equivalent circuit," *IEEE Trans. Magn.*, vol. 56, no. 3, Mar. 2020, Art. no. 7400608.

[10] N. Köster, O. König, and O. Bír ó, "Proper generalized decomposition with Cauer ladder network applied to eddy current problems," *IEEE Trans. Magn.*, vol. 57, no. 6, Jun. 2021, Art. no. 6300904.

[11] W. Chen, T. Henneron, S. Clénet, T. Delagnes, and J. Zou, "Model order reduction of an electro-quasistatic problem using CLN method," *Finite Elements Anal. Des.*, vol. 238, 2024, Art. no. 104185.

[12] L. Pace, N. Idir, T. Duquesne, and J.-C. D. Jaeger, "Parasitic loop inductances reduction in the PCB layout in GaN-based power converters using S-parameters and EM simulations," *Energies*, vol. 14, no. 5, 2021, Art. no. 1495.

[13] T. Henneron, S. Clenet, and F. Piriou, "Calculation of extra copper losses with imposed current magnetodynamic formulations," *IEEE Trans. Magn.*, vol. 42, no. 4, pp. 767–770, Apr. 2006.

[14] A. Bossavit, "Whitney forms: A class of finite elements for three-dimensional computations in electromagnetism," *Sci., Meas. Technol.*, vol. 135, no. 8, pp. 493–500, 1988.

[15] "GaN GS66502B (datasheet and model)." [Online]. Available: https://gansystems.com/gan-transistors/gs66502b/

Thomas Henneron received the graduation degree in electrical engineering and the doctoral degree in electrical engineering from the University of Lille, Lille, France, in 2001 and 2004, respectively.

Since 2006, he is an Associate Professor with the Laboratory of Electrical Engineering and Power Electronics (L2EP), University of Lille. His research interests include the development of the model order reduction approaches applied to FE models of electrical devices.

Wei Chen received the master's degree in nuclear engineering from Sun Yat-sen University, Guangzhou, China, in 2021. He is currently working toward the Ph.D. degree with the Arts et Métiers Sciences et Technologies, Paris, France.

His research interests include model order reduction for finite element models, specifically the Cauer Ladder Network method and Krylov subspace methods.

Loris Pace received the Ph.D. degree in electrical engineering from the University of Lille, Lille, France, in 2019.

He joined as an Associate Professor with the Ampere Laboratory and Ecole Centrale de Lyon, France, in 2021. His research interests include high and very high frequency power electronics, GaN power devices as well as high frequency characterization, and modeling of power systems.

Jérôme Tomezyk received the master's degree in applied mathematics from the University of Lille, Lille, France, in 2015, and the Ph.D. degree in mathematics with the Polytechnic University of Hauts-de-France, Valenciennes, France, in 2019.

His research interests include model order reduction for finite element models, particularly those related to electrical devices.

Stéphane Clénet received the doctoral degree in electrical engineering from INP Toulouse, Toulouse, France, in 1993.

He was an Assistant Professor with the University of Lille, Lille, France, in 1994 before being appointed in 2002 as a Full Professor of electrical engineering with Ecole Nationale Supérieure d'Arts et Métiers (ENSAM), France. He is working in the field of computational electromagnetics and its applications. His current research interests include ferromagnetic material modeling, model order reduction method, and uncertainty quantification.

Houssein Taha received the master's degree in applied mathematics from Lebanese University, Beirut, Lebanon, in 2017, and the Ph.D. degree in electrical engineering from the University of Lille, Lille, France, in 2021.

His research interests include the modeling and numerical simulation of high-frequency electromagnetic phenomena.